The effect of load thickness on the performance of high velocity, annular Z-pinch implosions

M. R. Douglas and C. Deeney
Sandia National Laboratory, Albuquerque, New Mexico 87185

N. F. Roderick
University of New Mexico, Albuquerque, New Mexico 87102

(Received 25 May 2000; accepted 28 September 2000)

Numerical calculations have been performed to investigate the role that load thickness may play in the performance of fast annular Z-pinch implosions. In particular, the effects of load thickness on the mitigation of the magnetically-driven Rayleigh–Taylor (RT) instability and energy coupling between the plasma load and generator are addressed. Using parameters representative of the Z accelerator [R. B. Spielman *et al.*, Phys. Plasmas **5**, 2105 (1998)] at Sandia National Laboratories, two-dimensional magnetohydrodynamic simulations show that increased load thickness results in lower amplitude, slightly longer wavelength RT modes. In addition, there appears to be an optimum in implosion velocity which is directly associated with the thickness of the sheath and subsequent RT growth. Thin, annular loads, which should couple efficiently to the accelerator, show a large reduction in implosion velocity due to extreme RT development and increased load inductance. As a consequence, thicker loads on the order of 5 mm, couple almost as efficiently to the generator since the RT growth is reduced. This suggests that Z-pinch loads can be tailored for different applications, depending on the need for uniformity or high powers. © *2001 American Institute of Physics.* [DOI: 10.1063/1.1327618]

I. INTRODUCTION

The magnetic implosion of thin cylindrical loads, or Z pinches, in the form of foils,[1] cylindrical gas puffs,[2,3] multiple shell gas puffs,[4,5] and both single and nested wire arrays,[6,7] has been used to produce dense hot plasmas for applications ranging from radiation material studies to inertial confinement fusion.[8–10] The ability to reach the temperatures and densities required for such applications depends strongly on the uniformity and symmetry of the pinch during the run-in phase of the implosion. These implosion characteristics can be severely degraded by the magnetohydrodynamic (MHD) Rayleigh–Taylor (RT) instability. This instability occurs at the plasma–magnetic field interface, resulting from the inward radial acceleration of the plasma shell by the magnetic field. Under certain conditions, this instability can rapidly become nonlinear, producing bubble–spike structures analogous to that observed in the nonlinear phase of the classic hydrodynamic RT instability. For finite plasma shells, the most destructive wavelengths are typically on the order of the shell thickness, a few mm.[11] As these modes continue to grow in amplitude, the entire load can become extremely distorted, leading to eventual bubble breakthrough of the plasma shell. This not only produces a broad and nonuniform pinch, but also disrupts current delivery by sending mass downstream of the main shell, preventing further acceleration of the load.

With the development of higher current, higher energy pulsed-power generators, some approaches in accelerator design (i.e., longer implosion times at larger masses) may require larger diameter loads to achieve peak implosion velocities comparable to those obtained on smaller generators. Such large diameter, high velocity implosions will be even more susceptible to the deleterious effects of nonlinear RT growth. For example, a standard wire array configuration on the Saturn[12] generator, which delivers approximately 8 MA of peak current with an implosion time of 50 ns, is between 7.5 mm to 12.5 mm in diameter. Typical implosion velocities (based on a 20:1 compression) range from 40 cm/μs to 100 cm/μs. With the Z generator,[13] which delivers approximately 1.8 MJ to the load and a peak current ranging from 16 to 20 MA, diameters ranging from 12.5 mm out to 40 mm diam are necessary.

Many techniques have been suggested to mitigate the RT growth in Z-pinch implosions, including uniform fill loads, i.e., uniform fill gas puffs,[14,15] the inclusion of shear flow,[16] and tailored density profiles[17] using multiple gas puffs or nested wire arrays. Previous analytic and numerical investigations of uniform fill loads, in particular, have proven to be quite promising in mitigating the RT development. However, such loads are known to be less efficient in coupling the electrical energy of the machine into thermal energy and subsequent radiation. To maximize radiation output, it is most desirable to capitalize on the stabilizing properties of uniform fill implosions, while maintaining the efficiencies observed with annular implosions. In this paper, we address this issue by exploring the transition from thin annular loads, such as wire arrays, to increasingly thicker plasma shells, which at present, could be approximately designed using gas puffs or nesting of annular loads. Such a systematic study is important since the optimum thickness for a *z* pinch shell is defined by the role of the various physics phenomena occurring as the shell thickness is increased.

In the following section, detailed two-dimensional (2D) magnetohydrodynamic calculations are presented for both aluminum and tungsten 40 mm diam loads, which have been varied in initial thickness and imploded at parameters characteristic of the Z generator. Based on these results, a correlation is shown to exist between implosion velocity and RT development. The details of this correlation and the physical mechanisms influencing it will be discussed in Sec. III. Section IV concludes with a load design based on the results of Secs. II and III and a simulation is shown for illustrative purposes. It should be stressed that the Z-pinch configurations in all of the calculations presented here are idealized and are not necessarily meant to represent loads that could be realized using wire arrays, gas puffs or low density foams. However, by simulating such loads, it is possible to quantify the role of RT development relative to geometric changes. Since a large number of experiments have been carried out on the Z generator with wire arrays comprised of different atomic elements, it was also of interest to repeat the simulations with two disparate atomic numbers. In this manner the influence of atomic number specifically on plasma resistivity could be quantified.

II. SHELL THICKNESS SURVEY

A series of calculations have been performed for a 40 mm diam, 20 mm high, 3.4 mg Z-pinch load with varying degrees of initial thickness. These calculations were carried out using the 2D MHD code MACH2 (Ref. 18) and are based on parameters *initially* characterized for Z. MACH2 is a time-dependent, single fluid, multitemperature, nonideal, radiation MHD code with Arbitrary Lagrangian/Eulerian (ALE) capability. The dynamic equations for the material density, electron and ion specific internal energies, radiation energy, velocity, and magnetic field are solved by the code in an operator split fashion. The equations are solved on a logical mesh composed of arbitrary quadrilateral cells with all physical processes but material advection calculated implicitly. Spatial differentiation is carried out using a finite volume differencing scheme. The equations of state and transport coefficients for the nonideal thermal and magnetic conduction exists in either an analytic form or a pregenerated tabular form, i.e., Los Alamos National Laboratory SESAME (Ref. 19) tables. In the latter case, the tables used are based on local thermodynamic equilibrium (LTE) plasma conditions. The radiation treatment includes both a simple emission model or a nonequilibrium, single group (3T) radiation diffusion model with opacity information obtained from SESAME tables.

For the calculations presented in this paper, the code was run in a purely Eulerian mode due to the severity of the RT growth. The vacuum region was approximated with a low density material (approximately three orders of magnitude lower) of the same composition as the load with a large constant electrical resistivity. A Spitzer analytic model was used for the thermal conductivity and magnetic resistivity in the load region, while SESAME data were used for equation of state parameters. Although the simulations were carried through stagnation on axis, the RT development was only considered during the run-in phase of the implosion. Consequently, the radiation emission model was implemented; this model is sufficient to describe the radiative losses during the run-in phase while the plasma remains optically thin and RT growth is dominated by the magnetohydrodynamics. This radiation model also drastically reduces computational run time compared to a 3T diffusion simulation.

The initial thickness of the Z-pinch load in the simulation ranged from 1 mm to 20 mm, where the latter distributes the plasma all the way to the stagnation axis, i.e., a uniform fill. The load was approximated by a uniform density, right circular cylindrical plasma shell with a temperature of 5 eV and an outer diameter of 40 mm. To seed the instability, a 5% random cell-to-cell density perturbation was superimposed throughout the shell; this was found to produce amplitude and wave structure comparable to that observed in previous Saturn experiments[16] and is thought to provide a phenomenological approximation to the seeding process believed to occur at initiation. Since aluminum and tungsten wire arrays are standard loads imploded on the Saturn and Z accelerators, these elements were considered as the load materials. Such different atomic numbers allow resistivity effects to be studied. It should be noted, however, that even at Z current levels there is insufficient mass to allow many of the load configurations here to be fabricated by any technique. To this end, aluminum and tungsten plasma shells as such were used for illustrative purposes. In each calculation, the total mass was nominally 3.4 mg, corresponding to initial densities of 1.35×10^{-4} g/cm^3 in the uniform fill limit to 1.35×10^{-3} g/cm^3 with the thin 1 mm shell.

The peak current delivered to the load ranged from 14 MA in the uniform fill case to 16 MA in the 1 mm annulus case. Such differences in current are due to the change in the inductance vs time histories of the loads. The current profile is shown in Fig. 1 along with the initial computational configuration for a 40 mm outer diameter, 1 mm thick load [Fig. 1(b)]. The electrodes which confine the top and bottom portion of the load are considered to be perfectly conducting walls. The numerical resolution in all calculations was kept constant at 0.125 mm axially and 0.2 mm radially, corresponding to 160 cells axially and 5 cells radially across the initial shell. This level of axial resolution ensured that wavelengths between 1 and 2 mm, which are often the most detrimental to the implosion dynamics, would be numerically resolved.[20]

The evolution of the 1 mm thick tungsten shell is displayed in Fig. 2 with isodensity contour plots at 90 ns, 100 ns, and 110 ns. This can be contrasted with the uniform fill load in Fig. 3, which is shown at similar stages in the implosion: 80 ns, 90 ns, and 100 ns. Clearly the calculational results demonstrate that as the initial shell or load thickness is increased, the nonlinear growth of the RT instability becomes less pronounced. Prior to stagnation, the 1 mm thick annular implosion is extremely unstable [Fig. 2(c)] while the pinch performance (as measured by the degree of uniformity) is dramatically improved with the uniform fill. In addition, a visual survey of the wavelength structure indicates that longer wavelengths are observed earlier in the uniform fill implosion compared to the thin shell; by 100 ns, the ob-

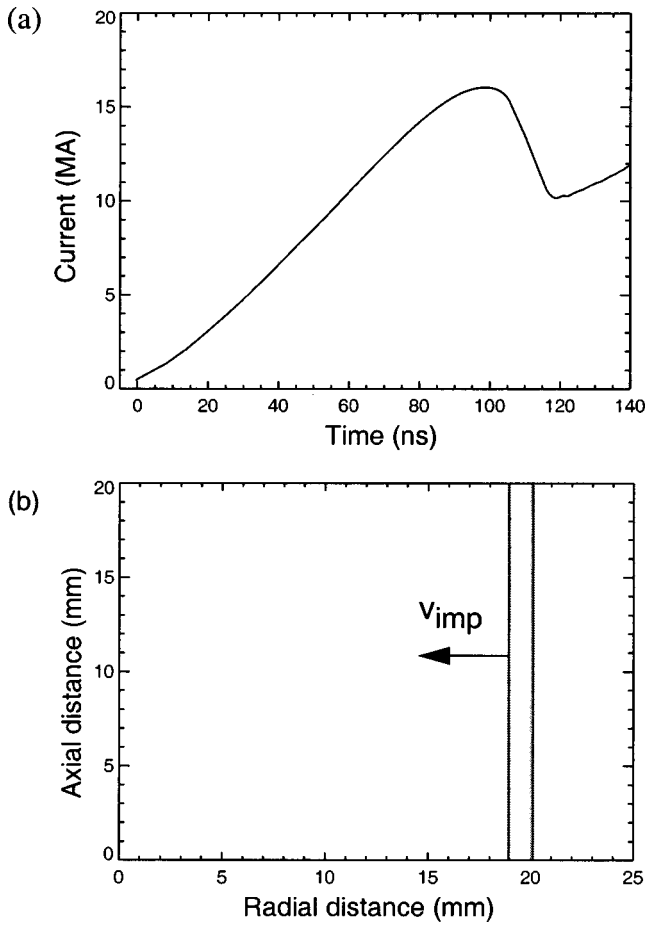

FIG. 1. (a) Current profile for a 40 mm diam, 1 mm thick load and (b) its initial simulated configuration. The load implodes toward the centerline defined by the left computational boundary. The top and bottom boundaries are considered to be perfectly conducting walls.

served wavelength is 1.54 mm in the uniform fill case compared to 1.18 mm with the 1 mm thick shell.

The RT structure and its evolution can be examined in more detail by performing a fast Fourier transform (FFT) of the perturbed region. This is shown in Figs. 4 and 5 which displays the FFT spectrum at the corresponding times of the density profiles of Figs. 2 and 3. Here, the spectrum was obtained using IDL,[21] by taking the FFT of the following:

$$\langle m\rangle(z)=\frac{\Sigma_i^n 2\pi\rho_{i,j}r_{i,j}dmr_{i,j}-\overline{m}}{\overline{m}},$$

where

$$\overline{m}=\frac{\Sigma_j^m[\Sigma_i^n 2\pi\rho_{i,j}r_{i,j}dmr_{i,j}]}{m}.$$

Here $\overline{m}$ is the axial averaged integrated radial mass and $\langle m\rangle$ is the deviation of that value at each axial position. There are a number of interesting features to note in the FFT spectra and evolution. Although a 5% random density seed was applied in both cases, the difference in densities resulted in similar initial spectra *but* with much lower average amplitudes in the uniform fill case (as a result of lower density). Previous simulations of Saturn experiments[16] with both uniform fill and annular gas puffs have reproduced the experimental data using the same initial random density seed; this suggests that a decrease in perturbation amplitude may actually occur experimentally and there may be a basis for keeping the initial perturbation seed constant in the simulations. Another interesting feature is that a faster transition to longer wavelengths is observed with the uniform fill even though the initial spectra is a lower average amplitude than that of the thin shell case.

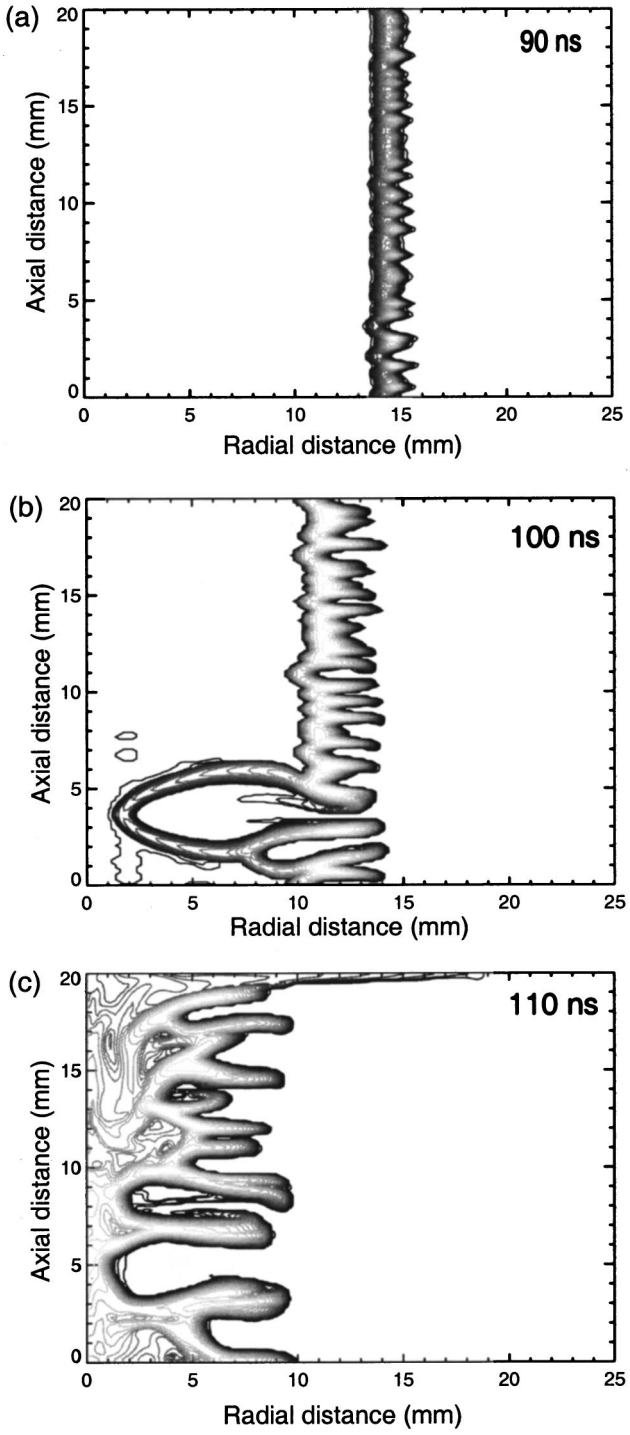

FIG. 2. Evolution of a 40 mm diam, 20 mm high, 1 mm thick annular tungsten load at (a) 90 ns, (b) 100 ns, and (c) 110 ns. The 4.0 mg load was seeded with an initial 5% cell-to-cell random density perturbation.

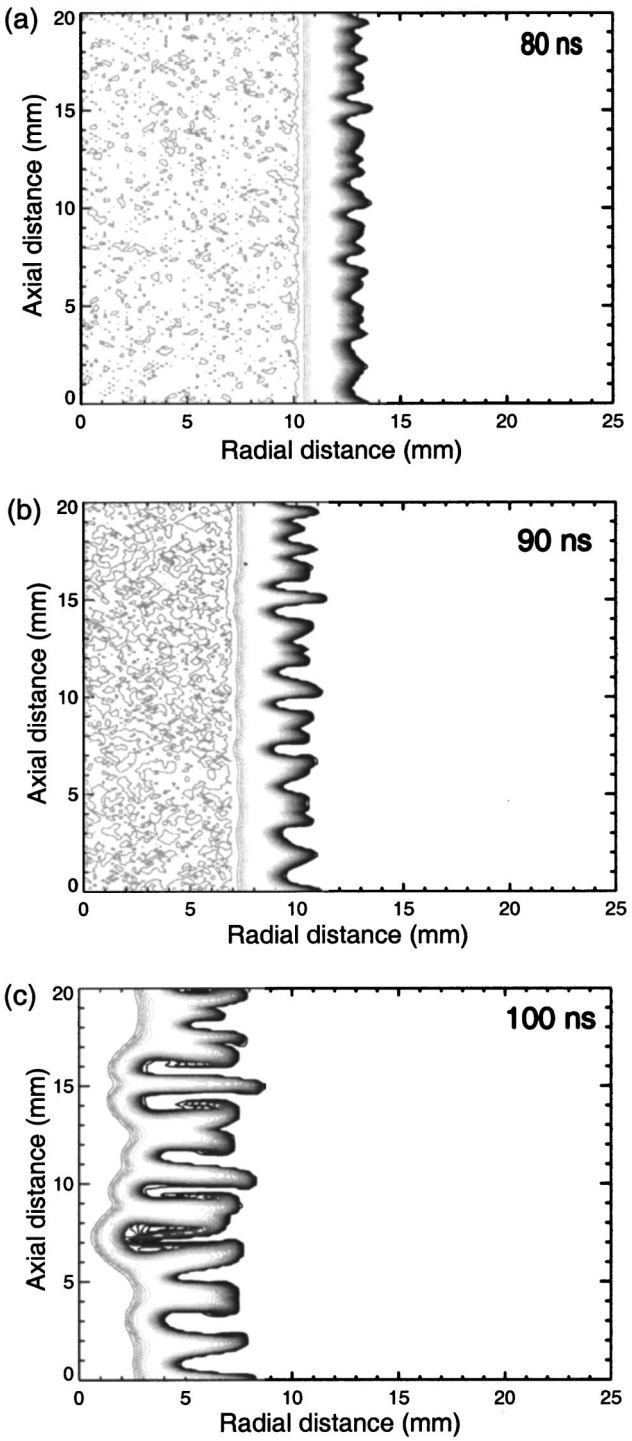

FIG. 3. Evolution of a 40 mm diam, 20 mm high, uniform fill tungsten load at (a) 80 ns, (b) 90 ns, and (c) 100 ns. The 4.0 mg load was seeded with an initial 5% cell-to-cell random density perturbation.

An explanation for the rapid transition to longer wavelengths with the uniform fill load is twofold. First, with the mass distributed over a broader shell, the RT interface is snowplowing (i.e., accreting mass) into a low density medium. The perturbation continues to evolve as short wavelengths transition to a slower growth rate, and are overtaken by longer wavelength structure. Furthermore, the uniform fill has a lower initial density and experiences a higher acceleration. This allows short wavelength structure to grow and saturate (both numerically and physically) on a faster time scale. The evolution is, of course, further complicated by mode coupling effects that may be occurring. This is in contrast to a thin shell, where at some wavelength, the perturbation does not saturate but instead continues to exponentiate.[20] In this sense, one would expect the thin shell case to always have more dominant short wavelength features in its FFT spectrum throughout the implosion. Nonetheless, long wavelength features do appear in this spectrum as well, as seen in Fig. 4. This is due in part to the large bubble development near the lower end of the pinch and a longer wavelength distortion developing throughout the pinch. This latter distortion may be caused by boundary conditions, mode coupling, or geometrical effects (in density profile). Although the transition to longer wavelengths occurs earlier in the implosion with the uniform fill, these wavelengths grow slower than their thin shell counterparts, as can be seen by comparing the spectrum at 90 ns in the uniform fill to that of the annular shell at 110 ns (where the RT interface is near the same radial position in the implosion).

Figure 6 compares isodensity contour plots for 2.5 mm, 5 mm, and 10 mm initially thick shells approximately 7 mm from the stagnation axis. As with the extreme cases of the 1 mm thin shell and uniform fill described above, a trend in RT development is evident. With the broader shells, the outer edge of the load must travel further through lower density material before reaching the stagnation axis. In such instances, the accumulation of plasma, particularly at the bubble surface, results in a decline in bubble velocity and evolution of longer mode structure. This can lead to a reduction of the RT growth during the nonlinear phase with only a minimal decrease in the radially directed bulk mass motion. From Fig. 6, it is apparent that the longer the accelerated RT front accretes upstream material, the longer the shell retains some semblance of uniformity. Another factor which may be playing a role in the RT reduction is the lowering of the magnetic driving force at the RT interface. This ''magnetic smoothing'' results from field diffusion into the extended plasma shell which reduces the current density in the region. This will be briefly addressed in the following section.

Results of the load thickness survey are summarized in Table I with peak current, implosion time, mass-averaged (bulk) peak radial velocity, and thermalization time for each load configuration listed. The implosion time was defined as the interval from initial current rise (taking the rise of the current profile and extrapolating to zero intercept) to peak radiated power; this approximated the time interval the load was in motion. The mass-averaged radial velocity, determined from the radial component of the momentum and the mass, is shown in Fig. 7 for the uniform fill [Fig. 7(a)] and the 1 mm thick shell [Fig. 7(b)], respectively. Here the velocity is plotted as a function of time, where zero time is the start of the current profile. The peak in the radial velocity is easily determined from these plots. The thermalization time was calculated from the peak radial velocity and the shell thickness (at the time of peak velocity), which is defined by the bubble–spike distance (approximately 10%–10% width of peak density).

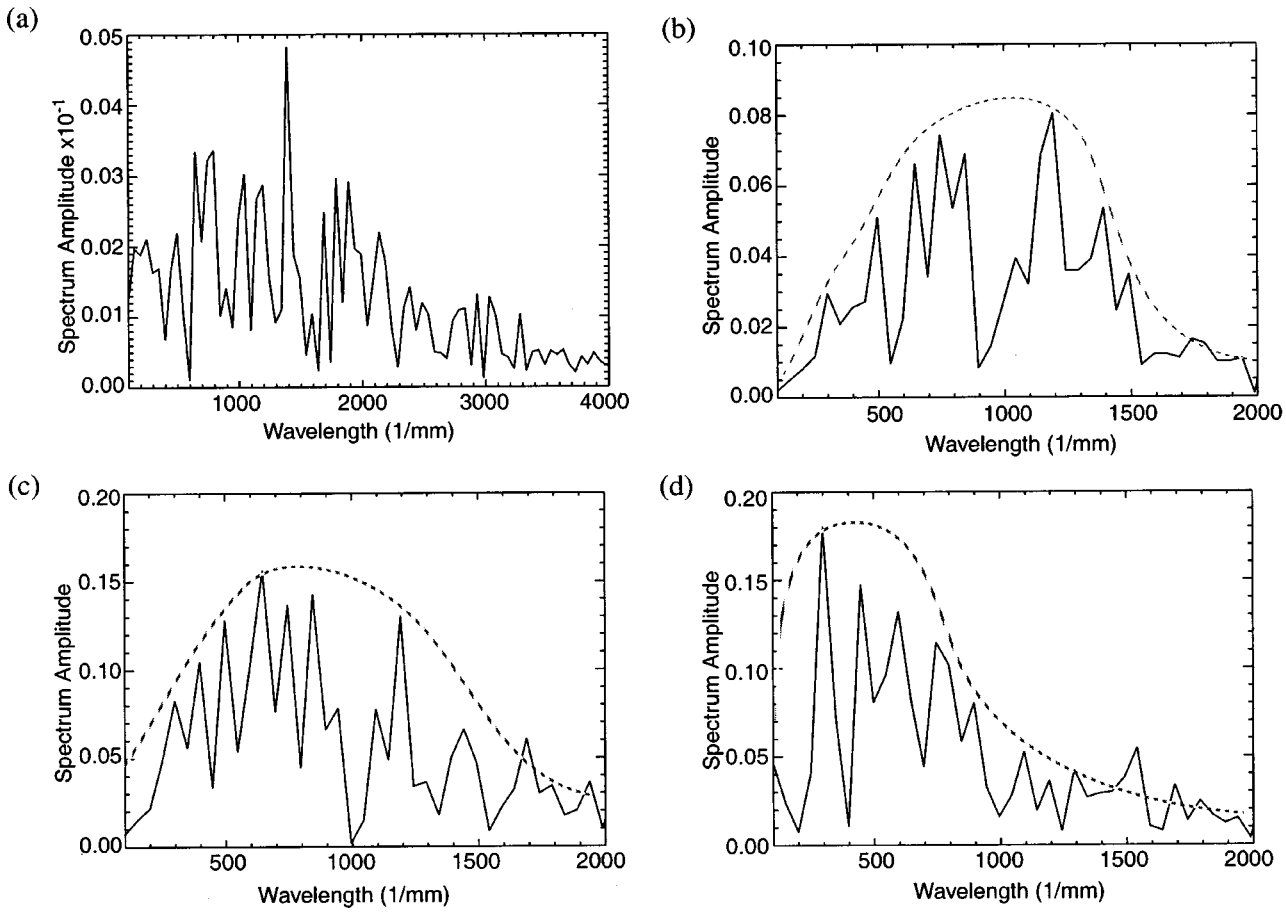

FIG. 4. The spectral evolution of the 1 mm thick load of Fig. 2. The spectrum is obtained by performing a FFT of the (a) initial shell and perturbed shell at (b) 90 ns, (c) 100 ns, and (d) 110 ns.

In addition to improved implosion uniformity, pinch performance is based on the coupling efficiency from machine to load. High efficiencies, which are manifest in large implosion velocities, are paramount to reaching high thermalization and radiation temperatures. However, calculations indicate that this efficiency may be dependent on the severity of the RT instability. This can be seen in Table I and is illustrated in Fig. 8. In this figure, the implosion velocity is plotted as a function of the load thickness for initially perturbed and unperturbed conditions for aluminum and perturbed conditions for tungsten. With the unperturbed loads, there is no initial density variation to seed the instability, and the implosions are uniform. The velocity is observed to monotonically increase with decreasing shell thickness due to improved coupling between the load and the driver. This trend is not seen with the initially perturbed loads. For a load thickness smaller than 10 mm, the velocity clearly deviates from what is observed with a uniform implosion. In fact, for the thinnest loads, the velocity remains between 40–50 cm/μs, far lower than the 70 cm/μs that would be seen with an ideal uniform thin shell. This decline in velocity is most likely associated with severe RT development in the later stages of the implosion as evident by the correlation between low velocity and large deviations from initial load thickness at late times (Figs. 8 and 6).

III. RT DEVELOPMENT AND IMPLOSION VELOCITY

The relationship between RT growth and peak implosion velocity is best understood by examining the details of the implosion physics. Computationally, initially thick loads are observed to mitigate RT growth. The visible wavelength structure tends to be longer and of lower amplitude (for same bulk mass radial location at late times) compared to that in the thin load implosions. Loads less than 10 mm thick are observed to be more susceptible to RT development since most of the shell mass is swept up in the early stages of the implosion. In this case, wavelengths on the order of the shell thickness grow quickly as bubble fronts encounter an ever increasing thinning material and the nonlinear RT bubble–spike structure is observed. The bubbles soon become broad and elongated, extending far beyond (i.e., towards the stagnation axis) what would have been the unperturbed plasma shell. The spikes, on the other hand, become long and thin, with magnetic field partially diffused into the high density regions (see Fig. 9). Compared to a uniform shell at the unperturbed plasma position, this former configuration is highly inductive. An examination of the current and density profiles in the extremely thin shell cases reveal highly distended current-carrying bubbles which stagnate much earlier than the bulk of the mass (which resides in the spike region).

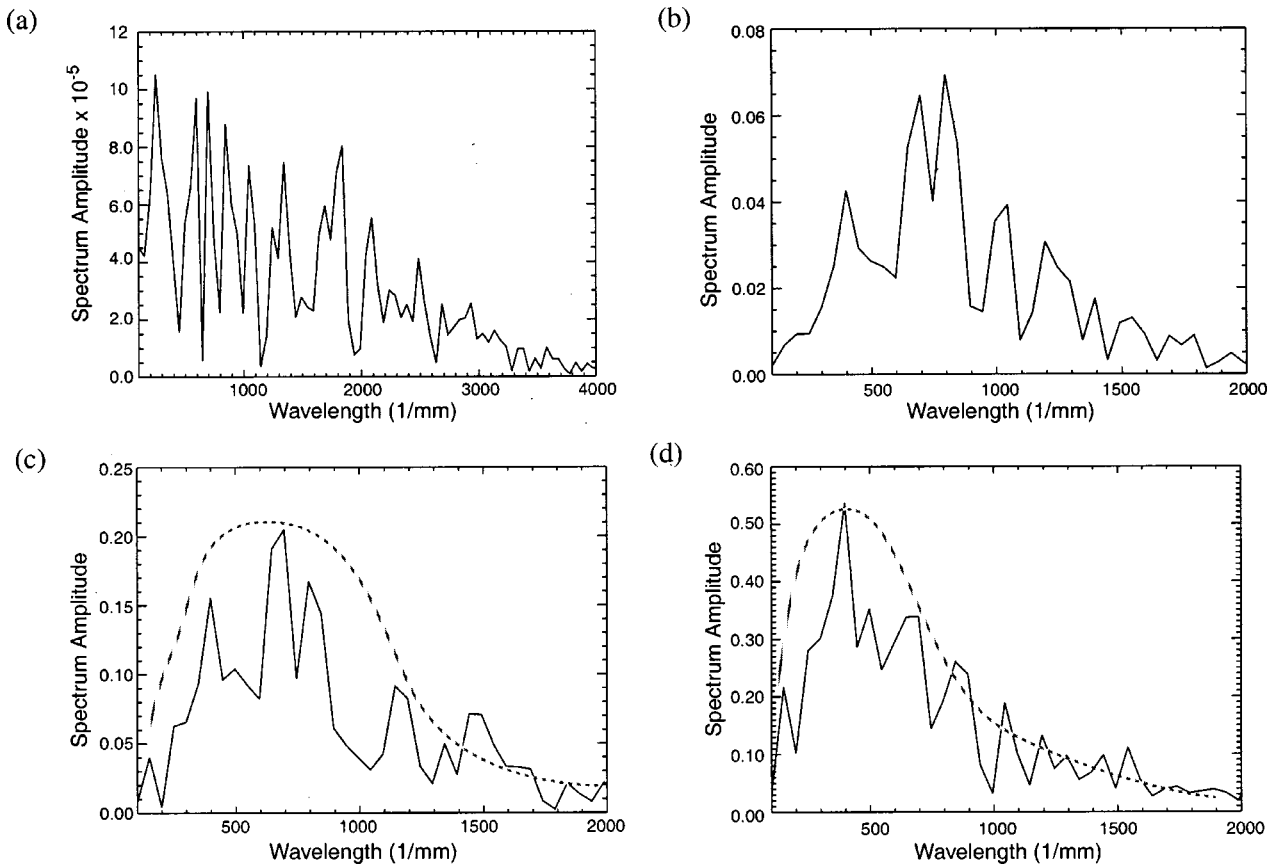

FIG. 5. The spectral evolution of the uniform fill load of Fig. 3. The spectrum is obtained by performing a FFT of the (a) initial shell and perturbed shell at (b) 80 ns, (c) 90 ns, and (d) 100 ns.

This corresponds to a loss of driving current at the bulk plasma–vacuum interface leading to a much lower velocity at stagnation. With the 5 mm and 7.5 mm shells, the bubbles ''run away'' much later in the implosion, after the peak current. As a consequence, there is less of an effect on the implosion velocity. Even with the 10 mm shell, which remains intact during the entire run-in, the instability influences the implosion velocity by introducing a slight change in inductance from bubble penetration into the downstream load plasma.

Based upon the observed correlation between RT development, load thickness, and velocity, one might expect the velocity to monotonically decrease with increasingly thin shells. In fact, in the extreme thin shell limit, a sharp drop (i.e., cliff) in velocity might be speculated since the plasma shell becomes so completely disrupted, there is minimal directional drive. An examination of Fig. 8 suggests that for the thin shell regimes (i.e., 1–5 mm) studied here, this precipitous drop is not observed. Instead the bulk velocity remains above 40 cm/μs. Computationally there is a reason for this enhanced velocity. Figure 10 compares a 1.5 mm initially thick aluminum load to that of a 1 mm thick load at 100 ns and 105 ns. Here, the current profile and density contour plots have been overlaid. By 105 ns into the implosion of the 1.5 mm load, Fig. 10(b), a large fraction of the current flow is in the low mass region ''blown'' ahead of the load as bubbles are pushed to the stagnation axis. This reduces the driving force in the bulk of the mass distribution residing in the spikes and the spikes nearly coast toward the axis. With the 1 mm load, the spikes are close enough, and there is enough low density material expanding between them, that current can flow across the narrow bubble regions, maintaining the driving force. This can be seen in Fig. 10(c) where, even though a large bubble has developed, the force on the bubble is reduced as current shorts across the bubble neck through the adjacent spike regions. By 105 ns, a small number of bubbles have stagnated on axis; however, there is still a continuous current flow across the spike regions defining the bulk of the plasma sheath and the velocity is observed to remain about the same. Although this continual ''healing'' occurs numerically and has been suggested theoretically,[22,23] it is not known whether this process takes place experimentally.

The influence of RT development on the final implosion velocity is observed to a lesser degree with loads broader than 10 mm. Although there is some RT growth, it is not enough to produce the large decline in velocity found with the thinner loads. As previously mentioned, the dominant mechanism for the RT mitigation in such cases is mass accretion, or snowplowing, into downstream material. With mass accretion alone, one can envision that a minimum density exists below which the accretion rate is insufficient to impede the RT development. This minimum required ''floor'' density can be determined to zeroth order by equating the force due to accrued mass (back pressure) at the

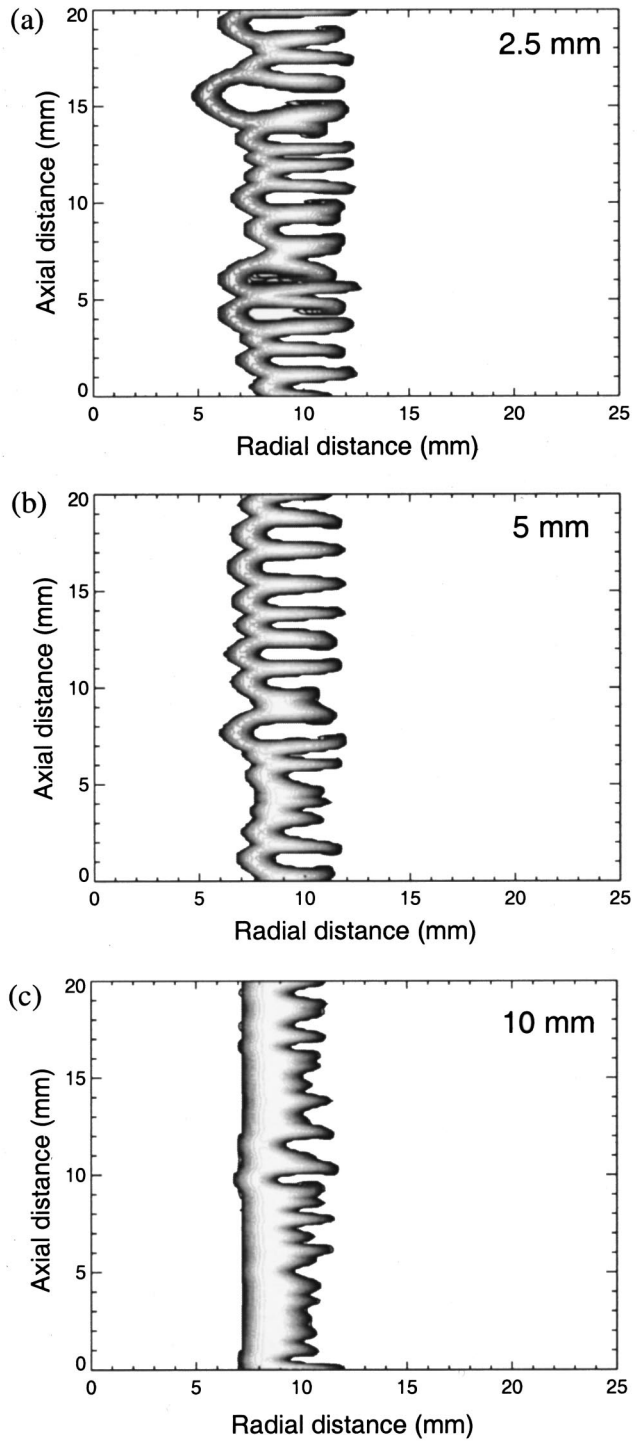

FIG. 6. Isodensity contour plots for a (a) 2.5 mm, (b) 5 mm, and (c) 10 mm load at approximately 7 mm from the stagnation axis.

bubble surface and the $J\times B$ accelerating force. For a right circular cylinder of height l, the mass that is swept up over a distance Δr of the implosion is given by $\rho(2\pi r\Delta r l)$. The rate of accretion is then

$$\dot{m}=\frac{m_{(\Delta r)}}{\Delta t}=\frac{m_{(\Delta r)}}{\Delta r}v=2\pi\rho r v l, \tag{1}$$

TABLE I. Results of the load thickness survey.

Load	I_{peak} (MA)	t_{impl} (ns)	V_P (cm/μs)	t_{thermal} (ns)
uniform	13.8	106	42.4	7
fill	(13.7)	(103)	(44.9)	(7)
Al, (W)				
1.5 cm	13.9	108	42.6	9
annulus	(13.9)	(105)	(43.8)	(8)
Al, (W)				
1 cm	14.6	109	47.2	9
annulus	(14.5)	(101)	(48.6)	(9)
Al, (W)				
7.5 mm	14.9	108	48.7	11
annulus		(106)	(46.9)	(15)
Al, (W)				
5 mm	15.3	10	48.4	13
annulus	(15.2)	(105)	(46.9)	(16)
Al, (W)				
2.5 mm	15.6	113	44.3	17
annulus		(106)	(46.5)	(17)
Al, (W)				
1.5 mm	15.8	108	45.9	18
annulus	(15.7)	(104)	(42.4)	(19)
Al, (W)				
1 mm	15.8	117	43.3	19
annulus	(15.7)	(113)	(46.6)	(19)
Al, (W)				

where v is the instantaneous implosion velocity. To slow bubble penetration into the load, the change in momentum, $\dot{m}v$, at the plasma–bubble interface should be on the order of the accelerating force. Approximating this by

$$\frac{\mu_0 I^2}{4\pi r}l, \tag{2}$$

an estimate for this floor density can be found,

$$\rho_{\text{floor}}=\frac{\mu_0 I^2}{8\pi^2 r^2 v^2}. \tag{3}$$

As an example, the floor density can be estimated for the 1 mm thick shell, 3.4 mg load simulation of Fig. 2. Values for current, velocity, and radius are taken from the simulation prior to extreme nonlinear RT development (i.e., amplitude approximately 0.75 λ). With the current at 15.6 MA, a velocity of 36.4 cm/μs and an imploding load at a radius of 10 mm, the minimum density required for RT mitigation is 1.9×10^{-4} g/cm^3. This value is a factor of 2 below the vacuum density defined in the calculations, and bubble breakthrough is observed during the run-in phase. By filling the interior region up to the stagnation axis with a low density fill at this floor value, the bubbles are prevented from becoming extremely distended prior to stagnation.

It should be noted that other physical mechanisms besides mass accretion may also reduce the RT growth in thick annular implosions and uniform fill loads. For high velocity implosions with supersonic flow, mass accretion is accompanied by a shock front propagating into the downstream low density material.[24] The degree to which this process influ-

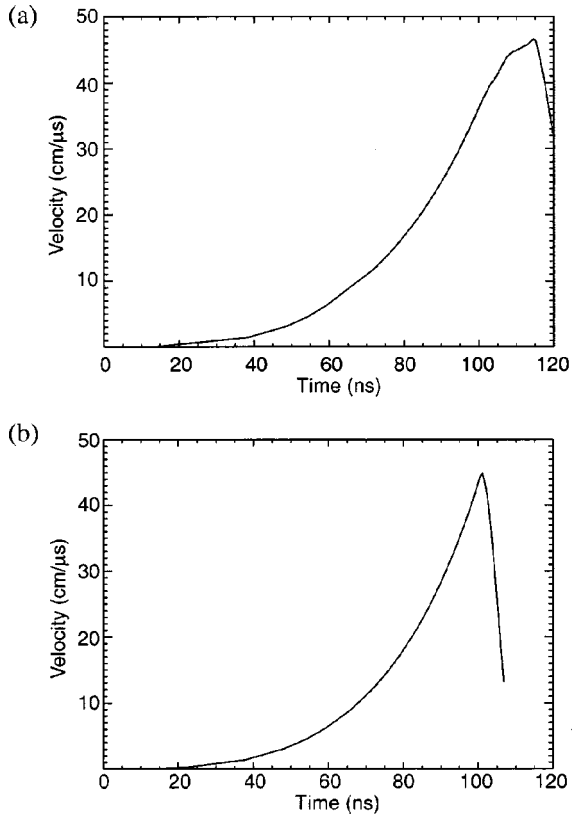

FIG. 7. The mass-averaged radial velocity as a function of time for (a) the thin 1 mm shell and (b) the uniform fill load.

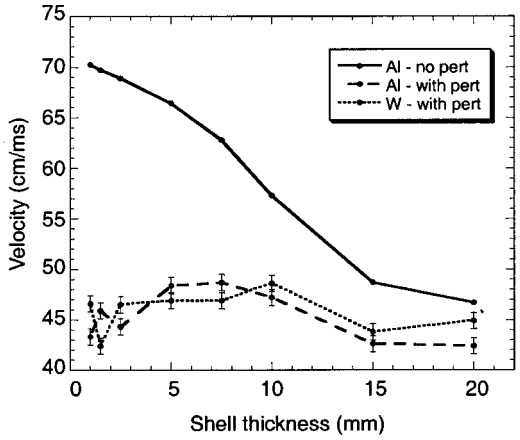

FIG. 8. Peak radial velocity as a function of load thickness for both aluminum and tungsten. The solid curve shows the results for an initially unperturbed aluminum implosion. The other two curves illustrate the trend observed when an initial 5% cell-to-cell random density seed is incorporated into the initial conditions.

ences the RT mitigation is not easily estimated and will not be discussed here. Another mechanism to consider is magnetic smoothing, as mentioned earlier. Figure 8 suggests that higher implosion velocities may be obtained for thicker loads with higher atomic number materials, such as tungsten (compare tungsten and aluminum velocities). This improvement in velocity is thought to be the result of magnetic smoothing, an effect by which the magnetic pressure is lowered at the RT interface due to the diffusion of magnetic field into the unperturbed load regions upstream. With $\eta \propto \overline{Z} T_e^{-3/2}$, where η is the spitzer electrical resistivity, $\overline{Z}$ is the mean ionization state, and T_e is the electron temperature, the magnetic field can diffuse further into a tungsten load compared to aluminum. This reduces the current density in the RT region which in turn lowers the magnetic pressure ($J \times B$ force) on the bubble front, hence slowing nonlinear RT development. This is illustrated in Fig. 11 which shows the diffusion of magnetic field into a uniform fill load early in the implosion for both tungsten and aluminum [Fig. 11(a)]. For tungsten, $\overline{Z}$ is ~ 8 compared to 4 for aluminum and the field diffuses more rapidly into the tungsten shell. The effect of this diffusion on velocity is shown in Fig. 11(b).

While magnetic smoothing is a likely candidate for the observed differences between aluminum and tungsten velocities with thick shells, the importance of this effect is most evident by considering an ideal MHD case, where resistive effects are not included. This is demonstrated in Fig. 12 where tungsten uniform fill simulations, with and without resistive diffusion, are shown at 90 ns into the implosion. A dramatic decline in pinch quality is observed in the case devoid of field penetration into the unperturbed plasma. Note that the wavelength structure has only been modified in amplitude; the same RT modes develop, but more swiftly. This amplitude modification results in a reduction of the peak implosion velocity from 44.9 cm/μs down to 34.9 cm/μs.

The explanation of magnetic smoothing given for thick loads naturally does not apply as the shells become thinner. Indeed, Fig. 8 shows the tungsten implosion velocity as slightly lower than the aluminum velocity for 5 mm to 1 mm thick loads. The reason for this is not well understood. One speculation is that the tungsten radiates more efficiently during the run-in phase, and as a result, the bubbles fronts have less resistance and are able to grow faster. Another argument may be that within the error bars on the velocity (defined by the linear interpolation on velocity data), there is actually little or no differences. In any case, the trend between the two different materials is the same; there is a strong correlation between RT development, load thickness, and peak implosion velocity.

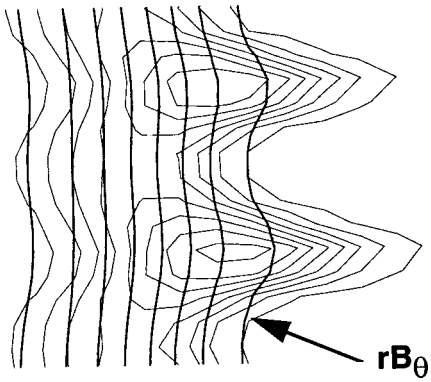

FIG. 9. Overlay of isodensity contour plot and rB for the 1 mm annular implosion at the early stages of nonlinear growth.

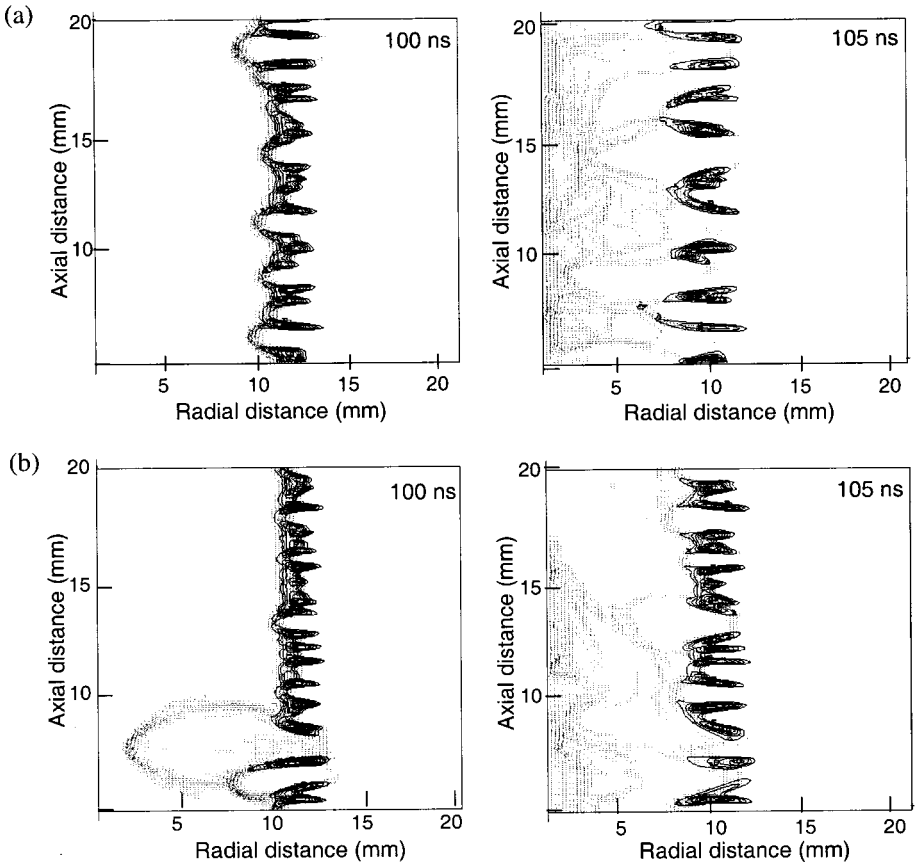

FIG. 10. Overlay of current density and isodensity contour plots for the (a) 1.5 mm and (b) 1 mm load at 100 and 105 ns into the implosion.

IV. THE TUNING LAYER LOAD DESIGN

The results of Secs. II and III show that increased shell thickness in annular Z pinch implosions can aid in reducing early-time nonlinear RT growth. In addition to improved pinch quality, the analysis suggests that for shells thicker than 5 mm, there is little reduction in achieved velocities. There are fabrication issues involved with making such thick loads, however, particularly with tungsten. To utilize the mitigating effect of mass accretion observed with thick shells, an interior shell can be imposed downstream of the initial thin load. This inner load, or tuning layer, combined with the initial load approximates a thick shell. Optimization of such a configuration could lead to enhanced pinch performance otherwise not attainable.

The criteria developed for the variable thickness cases of the previous section can be applied to the tuning layer concept. This is shown in Fig. 13 for a 3.4 mg, 40 mm diam, 1 mm thick tungsten annular load. In this case, a 5 mm thick tuning layer as opposed to a full interior fill was incorporated into the load design. The floor density was determined from the calculational parameters for the single load at 90 ns. With a current of 15.4 MA, a velocity of 24.9 cm/μs, and a radius of 14 mm, this minimum value was found to be 3.2×10^{-4} g/cm^3. The tuning layer was placed so that its front edge was at a radius of 10 mm as shown in Fig. 13. From the figure, it is clear that the tuning layer improves the implosion stability at late times in the implosion. At a distance of 5 mm from the stagnation axis, the tungsten annular load has a velocity of 45 cm/μs. The tungsten annular load/tuning layer has a combined mass of 5.9 mg and a velocity of 37 cm/μs. Here pinch uniformity was drastically improved while the velocity dropped by 10%.

The tuning layer design presented in Fig. 13 was one approach at developing a useful load configuration. Obviously, the configuration used in an experiment should be optimized for the type of load (i.e., wire arrays, gas puffs, foams) and accelerator. Such a procedure was recently carried out on Z by utilizing a nested wire array geometry.[7] This design brought about a 20% enhancement in peak power over a single array design. It should be noted that Hussey *et al.*[25] have examined nonlinear RT growth in annular implosions with a heuristic model treating mass ejection from bubble regions to spikes. Based on their formulation for mass loss, an alternative estimate for the floor density could also be obtained by requiring that the ejected mass from bubble regions be replenished by accreted mass during run-in.

V. CONCLUSIONS

Radiation MHD calculations have been carried out to investigate the role of initial load thickness on RT development and subsequent pinch performance. For example, uniform fill loads, such as gas puffs, have been experimentally and computationally shown to mitigate RT growth. However, they are known to couple energy less efficiently from the pulsed-power driver than thin annular loads. To examine the trade-off between coupling and RT mitigation, parameters indicative of the Z accelerator at Sandia National Labo-

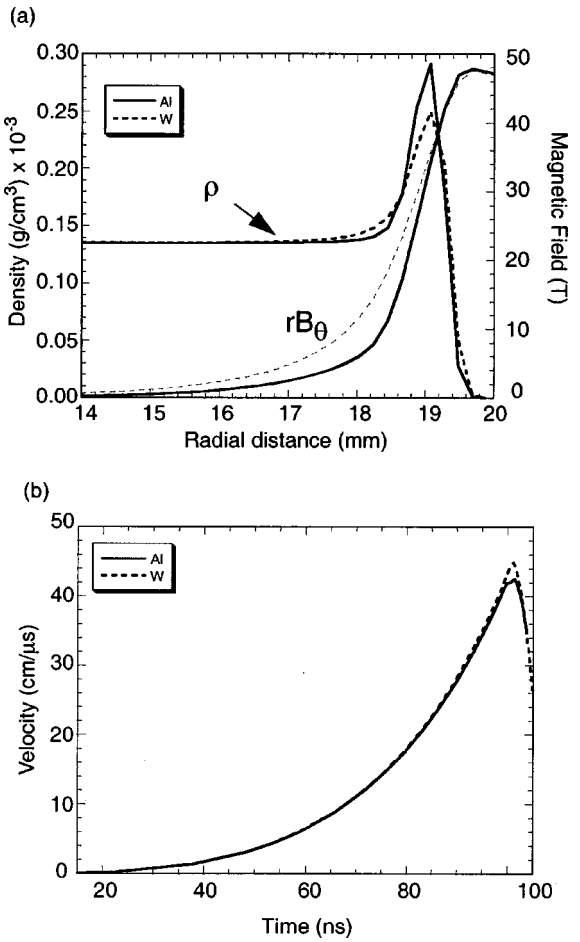

FIG. 11. (a) Overlay of density and rB profiles as a function of radial distance for both aluminum and tungsten uniform fill loads early in the implosion and (b) the corresponding implosion velocities.

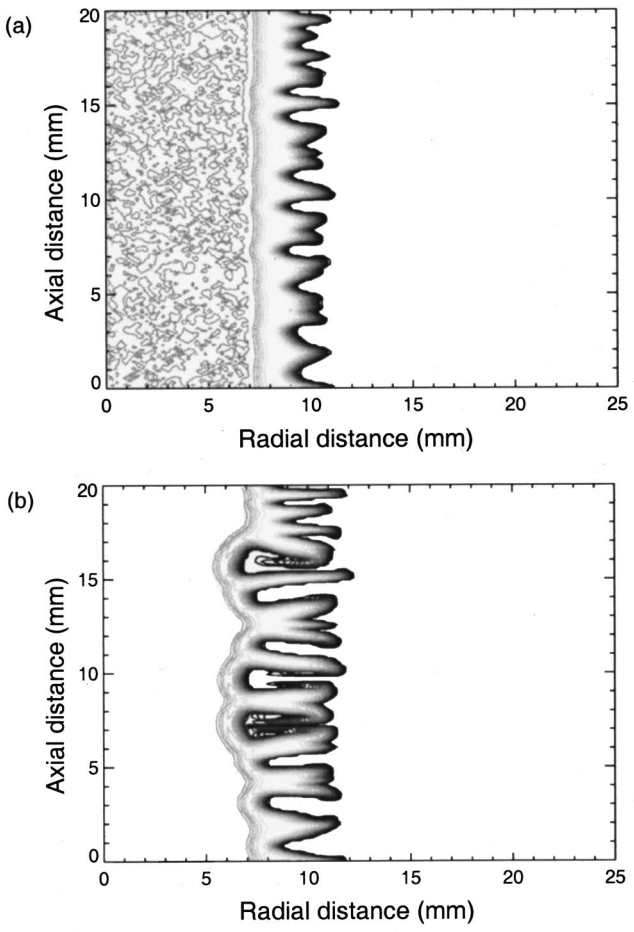

FIG. 12. Tungsten uniform fill implosion at 90 ns (a) with resistive diffusion and (b) without resistive diffusion (ideal MHD).

ratories were used to implode a 40 mm diam load ranging in thickness from 1 mm up to 20 mm (uniform fill). A 5% cell-to-cell random density was used to seed the initial perturbation. Simulations indicate that the efficiency believed to occur with thin annular shells is reduced because of extreme RT development. In this case, the initially thin load becomes highly distorted from bubble–spike development during the later stages of the implosion. The result is a higher inductance, lower velocity configuration.

Although the thin loads were observed to decrease significantly in velocity when compared to an unperturbed case, i.e., 40 cm/μs compared to 60–70 cm/μs, the velocity never dropped below 40 cm/μs. Computationally, this was related to a current ''healing'' effect at the neck of the bubble regions. With the thinner loads, the spike-to-spike distance was small enough and thermal expansion of the low density surrounding plasma high enough, that current could eventually conduct across the low density gaps (bubble neck) between some spikes. This transfer of current from the bubble front to the bubble neck reduced the magnetic pressure on the bubble itself, maintaining the driving force on the bulk of the mass carried by the spikes. For the calculations performed on both aluminum and tungsten loads with an initial thickness between 1 and 5 mm, the occurrence of this connection depended on the proximity of spikes and could be quite random. This continual ''healing'' has been suggested theoretically; however it is not known whether this process takes place experimentally.

The physical mechanisms that were discussed in this paper to reduce RT growth in thick loads included both mass accretion and magnetic smoothing. Mass accretion, or snowplowing in the supersonic case, is the primary method of impeding RT growth. However, magnetic smoothing can also play a strong role. In broad shells, where the field can diffuse far into the upstream material, the magnetic pressure is lowered or *smoothed* at the RT interface. This initially reduces the drive on the bubble slowing nonlinear RT development. This effect is most noticeable when a comparison is made to an ideal MHD calculation, where resistive effects are not important. Magnetic smoothing can also be seen when transitioning to higher Z materials; the differences observed in this case are small, but may be important.

Based on the analysis presented in this paper, an optimum regime in performance may be inferred by considering both the velocity dependence on initial shell thickness and the need to minimize RT growth. For applications that require a high degree of axial uniformity with less emphasis on velocity, the optimum regime to consider ranges from a shell thickness of 5 mm to a uniform fill. In situations that require

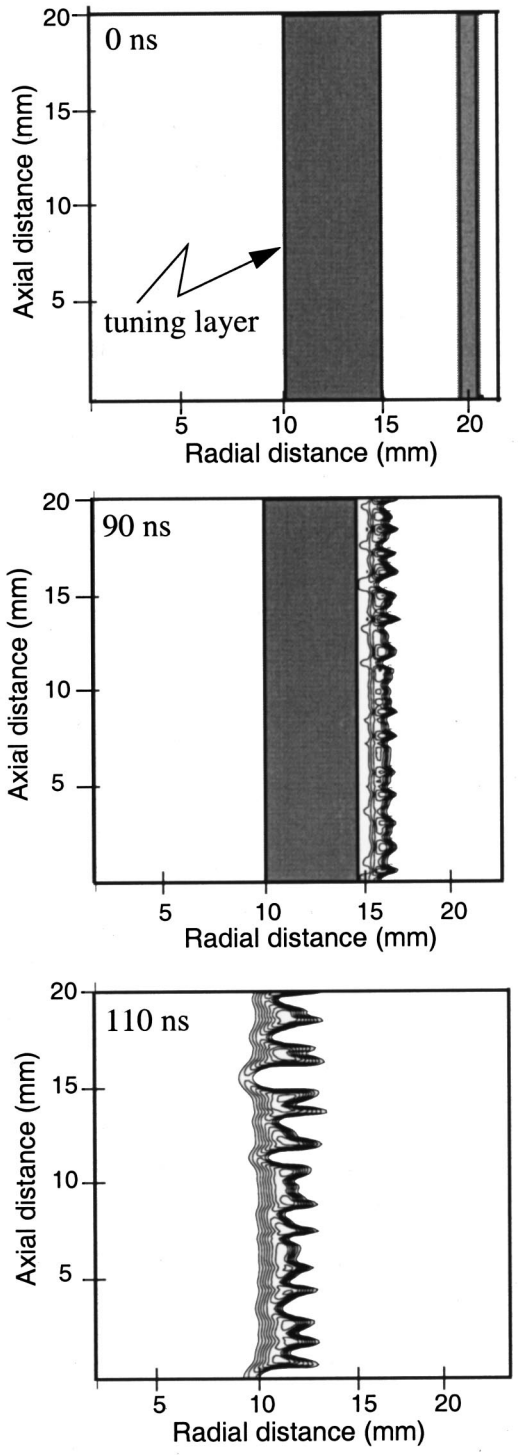

FIG. 13. The introduction of a nested shell downstream of a 1 mm thick, 40 mm diam annular load (similar to that of Fig. 2) leads to improvements in pinch quality. Using a floor density estimate, a 5 mm thick inner shell is placed at 20 mm diam. Isodensity contour plots are shown at 0 ns, 90 ns, and 110 ns into the implosion. The combined array mass is 5.9 mg and the peak radial velocity is 37 cm/μs.

high velocities, the appropriate range would be from 2.5 mm to 5 mm. At these widths, the velocities are near optimum values, while the degree of the instability may be acceptable. Although these calculations are specific to a 40 mm diam load on the Z machine, this analysis, which shows the trade-off between RT growth and achieved velocities, can be applied to any load design. To attain the optimum load performance for the 40 mm case requires either gas puffs or the development of lower density foams. Both of these options are limited: with gas puffs, the axial variations are difficult to control, while the manufacturing and machining of sub-10 mg/cm^3 density foams are not fully developed. Thicker shells will be easier to realize on future, high current generators. For the present experiments, this may be approximated by multiple shell configurations. Experimentally, this has been carried out for a two-nested wire array configuration[7] and two and three shell gas puffs.[4,5]

ACKNOWLEDGMENTS

We would like to acknowledge beneficial discussions with Sasha Velikovich, Ted Cochran, and Darrell Peterson. Sandia is a multiprogram laboratory operated by Sandia Corporation, a Lockheed Martin Company, for the United States Department of Energy under Contract No. DE-AC04-94AL85000.

[1]W. Matuska, R. L. Bowers, J. H. Brownell *et al.*, Phys. Plasmas **3**, 1415 (1996).
[2]R. B. Spielman, D. L. Hanson, M. A. Palmer *et al.*, J. Appl. Phys. **57**, 830 (1985).
[3]C. Deeney, P. D. LePell, F. L. Cochran *et al.*, Phys. Fluids B **5**, 992 (1993).
[4]R. B. Baksht, I. M. Datsko, V. I. Oreshkin *et al.*, Fiz. Plazmy **22**, 622 (1996) [Plasma Phys. Rep. **22**, 563 (1996)].
[5]V. Smirnov, Plasma Phys. Controlled Fusion **33**, 1697 (1991).
[6]T. W. L. Sanford, G. O. Allshouse, B. M. Marder *et al.*, Phys. Rev. Lett. **77**, 5063 (1996).
[7]C. Deeney, M. R. Douglas, R. B. Spielman *et al.*, Phys. Rev. Lett. **81**, 4883 (1998).
[8]C. Deeney, C. A. Coverdale, M. R. Douglas *et al.*, Phys. Plasmas **6**, 2081 (1999).
[9]M. K. Matzen, Phys. Plasmas **4**, 1519 (1997).
[10]J. H. Hammer, M. Tabak, S. C. Wilks *et al.*, Phys. Plasmas **6**, 2129 (1999).
[11]T. W. Hussey and N. F. Roderick, Phys. Fluids **24**, 1384 (1981).
[12]C. Deeney, T. J. Nash, R. B. Spielman *et al.*, Phys. Rev. E **56**, 5945 (1997).
[13]R. B. Spielman, C. Deeney, G. A. Chandler *et al.*, Phys. Plasmas **5**, 2105 (1998).
[14]F. L. Cochran, J. Davis, and A. L. Velikovich, Phys. Plasmas **2**, 1 (1995).
[15]N. F. Roderick, R. E. Peterkin, Jr., T. W. Hussey *et al.*, Phys. Plasmas **5**, 1477 (1998).
[16]M. R. Douglas, C. Deeney, and N. F. Roderick, Phys. Rev. Lett. **78**, 4577 (1997).
[17]A. L. Velikovich, F. L. Cochran, J. Davis *et al.*, Phys. Plasmas **5**, 3377 (1998).
[18]Robert E. Peterkin Jr., Michael H. Frese, and Carl R. Sovinec, J. Comput. Phys. **140**, 148 (1998).
[19]See National Technical Information Service Document No. DE94-011699 (J. D. Johnson, ''SESAME Data Base''). Copies may be ordered from the National Technical Information Service, Springfield, Virginia 22161.
[20]M. R. Douglas, C. Deeney, and N. F. Roderick, Phys. Plasmas **5**, 4183 (1998).
[21]*IDL Reference Guide* (Research Systems, Inc., Boulder, CO, 1992).
[22]D. L. Peterson, R. L. Bowers, K. D. McLenithan *et al.*, Phys. Plasmas **5**, 3302 (1998).
[23]J. DeGroot (private communication, 1999).
[24]S. M. Gol'berg and A. L. Velikovich, Phys. Fluids B **5**, 1164 (1993).
[25]T. W. Hussey, N. F. Roderick, U. Shumlak *et al.*, Phys. Plasmas **2**, 2055 (1995).